Data Article

Heat transfer data of two-phase flow in a horizontal tube filled with metal sponge

Sonja WEISE, Sarah KLEIN, Raquel ORIAS CALVO, Franziska MÜLLER-TREFZER, Thomas WETZEL, Benjamin DIETRICH

Karlsruhe Institute of Technology, Institute of Thermal Process Engineering (TVT), Kaiserstr. 12, Karlsruhe, Germany

Abstract

Experimental data on the heat transfer coefficient during saturated flow boiling of CO_2 in a horizontal cylindrical tube (diameter 14 mm) with integrated metal sponges (open-cell metal foams) are presented in this publication. The nominal cell density of the sponges was 10 ppi ("pores per inch") or 20 ppi. The mass flux varied from 25 kg m^{-2} s^{-1} to 125 kg m^{-2} s^{-1} and the vapor quality from 10% to 100%. The saturation pressure was either 12 bar, 19 bar or 26.5 bar. The length filled with sponge upstream of the heated part of the test section was 38 mm for the 10 ppi sponge and either 35 mm or 135 mm for the 20 ppi sponge. For the 20 ppi sample, the proportion of the test section filled with sponge was varied to investigate entrance effects. As a reference, the heat transfer coefficient during flow boiling in the empty tube was determined. In addition, geometric properties of the sponges relevant for the heat transfer coefficient (window diameter, strut diameter, porosity, specific surface area, and heat conductivity), were identified.

In der hier vorgestellten Publikation werden experimentelle Daten zum Wärmeübergangskoeffizienten beim gesättigten Strömungssieden von CO_2 in einem horizontalen zylindrischen Rohr (Durchmesser 14 mm) mit integrierten Metallschwämmen (offenzellige Metallschäume) präsentiert. Die nominelle Zelldichte der Schwämme betrug 10 ppi („Poren pro Zoll") bzw. 20 ppi. Der Massenstrom wurde von 25 kg m^{-2} s^{-1} bis 125 kg m^{-2} s^{-1} variiert, der Strömungsdampfgehalt lag zwischen 10% und 100%. Der Sättigungsdruck betrug entweder 12 bar, 19 bar oder 26,5 bar. Die mit Schwämmen gefüllte Länge stromaufwärts der beheizten Zone betrug 38 mm beim 10 ppi Schwamm und entweder 35 mm oder 135 mm beim 20 ppi Schwamm. Für die 20 ppi Probe wurde der Anteil des mit Schwamm gefüllten Testabschnitts variiert, um Einlaufeffekte zu untersuchen. Als Referenz wurde der Wärmeübergangskoeffizient während des Strömungssiedens im leeren Rohr bestimmt. Darüber hinaus wurden die für den Wärmeübergangskoeffizient relevanten geometrische Eigenschaften der Schwämme (Fensterdurchmesser, Stegdurchmesser, Porosität, spezifische Oberfläche und Wärmeleitfähigkeit) ermittelt.

Contact: benjamin.dietrich@kit.edu; thomas.wetzel@kit.edu

Specifications table

Subject area	Engineering, two-phase fluid flow through porous media, flow boiling
Type of data	Excel table
How data was acquired	Flow boiling test facility at the Institute of Thermal Process Engineering, Karlsruhe Institute of Technology
Data format	Analyzed
Experimental factors	<u>Sponges</u> 10 ppi copper sponge made by replication technique • total porosity: 91% • open porosity: between 85% and 88% • nominal cell density: approximately 10 pores per inch • mean strut diameter: 0.45 mm • mean window diameter: 1.6 mm 10 ppi plastic sponge made by 3D printing • total and open porosity: 86% • nominal cell density: approximately 10 pores per inch • mean strut diameter: 0.6 mm • mean window diameter: 2.0 mm 20 ppi copper sponge made by replication technique • total porosity: 90% • open porosity: between 84% and 87% • nominal cell size: approximately 20 pores per inch • mean strut diameter: 0.28 mm • mean window diameter: 1.0 mm <u>Operating conditions</u> two-phase flow boiling in test section filled with sponges • pressure: 12 bar, 19 bar and 26.5 bar • mass flux: 25 kg m^{-2} s^{-1} to 125 kg m^{-2} s^{-1} • vapor quality: 10% to 100% • heat flux: 3 kW m^{-2} to 65 kW m^{-2} • boundary condition: constant wall temperature, constant wall heat flux two-phase flow boiling in empty tube • pressure: 12 bar and 26.5 bar • mass flux: 25 kg m^{-2} s^{-1} to 150 kg m^{-2} s^{-1} • vapor quality: 10% to 100% • heat flux: 1 kW m^{-2} to 40 kW m^{-2} • boundary condition: constant wall temperature, constant wall heat flux

Data sets

sponge type	identifier	length of sponge upstream of heated section / mm	length of sponge in heated part of test section / mm	number of data points
empty tube	et.T; et.T.rep; et.q	-	-	78
10 ppi	10.T; 10.T.rep; 10.q	195	200	115
20 ppi	20.T; 20.T.rep; 20.q	135	195	151
20 ppi	20.T.sh	35	195	31
20 ppi	20.q.pm2	-	87	17
20 ppi	20.q.pm3	-	37	15

Experimental features	Flow boiling test facility with test section (horizontal tube, diameter 14 mm, heated length: 195 mm) especially designed to observe the heat transfer coefficient, the pressure drop, and the flow pattern at a specific mass flux, vapor quality, saturation pressure, and heat flux
Data source location	Repository KITopen

Value of the Data

- data can be used to validate models describing the heat transfer coefficient during flow boiling in consolidated porous media, i.e. sponges
- data can be used to derive the influence of geometrical properties of the sponges
- data can be used to assess the efficiency of integrating metal sponges into horizontal evaporator tubes for enhancing flow boiling processes

Data

The heat transfer coefficient during flow boiling of carbon dioxide (CO_2, R744, purity grade 4.5) flowing through two different copper sponge samples integrated into a horizontal tube with an inner diameter of 14 mm, is presented. The copper sponge samples featured a) a total porosity of 91% and an approximate nominal cell density of 10 ppi ("pores per inch") and b) a total porosity of 90% and an approximate nominal cell density of 20 ppi. The heat transfer coefficient during flow boiling in the empty tube is presented for comparability and validation of the test section. In case of the 20 ppi sponge, the length upstream of the heated zone and the proportion of the heated zone which was filled with sponge was varied to evaluate entrance effects. The 10 ppi copper sponge covered only the heated zone of the test section, the rest was filled with a similar plastic sponge.

The mass flux, $\dot{m}$, the vapor quality, $\dot{x}$, and the saturation pressure, p, of each data point are specified. The heat flux, $\dot{q}$, related to inner surface area of tube in the heated zone, is presented as well. Measurements with the same mass flux, vapor quality and saturation pressure were carried out with successively decreasing heat flux. Such a set of successive measurements is referred to as "measurement series" hereinafter. Several measurement series were repeated on different days to test the repeatability. The data of the repeatability measurements are presented as well. The extended measurement uncertainty (coverage factor k=2), 2σ, and the standard deviation of 40 subsequent data points, s, are reported. All heat transfer coefficient measurements presented in this paper were carried out at the flow boiling test facility of the Institute of Thermal Process Engineering (TVT) at KIT [1–5] using the test section described in this paper. The measurements were conducted at saturation pressures of 12 bar, 19 bar and 26.5 bar (corresponding to saturation temperatures of -35 °C, -21 °C and -10 °C, respectively), a mass flux between 25 kg m^{-2} s^{-1} and 125 kg m^{-2} s^{-1}, a vapor quality of 10% to 100% and a circumferentially averaged heat flux of up to 65 kW m^{-2}.

Experimental Design, Materials, and Methods

The description of the test facility and the test section is similar to the description published earlier [6], now focusing on the measurement of the heat transfer coefficient instead of the pressure drop.

Test facility

A process flow diagram of the TVT flow boiling test facility is shown in Fig. 1. Pure CO_2 (purity grade 4.5), stored in a tank, is subcooled and pumped into the test loop. The mass flow rate of the subcooled liquid is measured by a Coriolis mass flow meter (Promass F 60 by Endress+Hauser AG) and adjusted with an electronic control valve. Three pre-heaters in series adjust the vapor quality in the middle of the test section according to an enthalpy balance. The last pre-heater upstream of the test section is a smooth tube with the same inner diameter as

the test section. Downstream of the test section, a sight glass enables the observation of flow patterns.

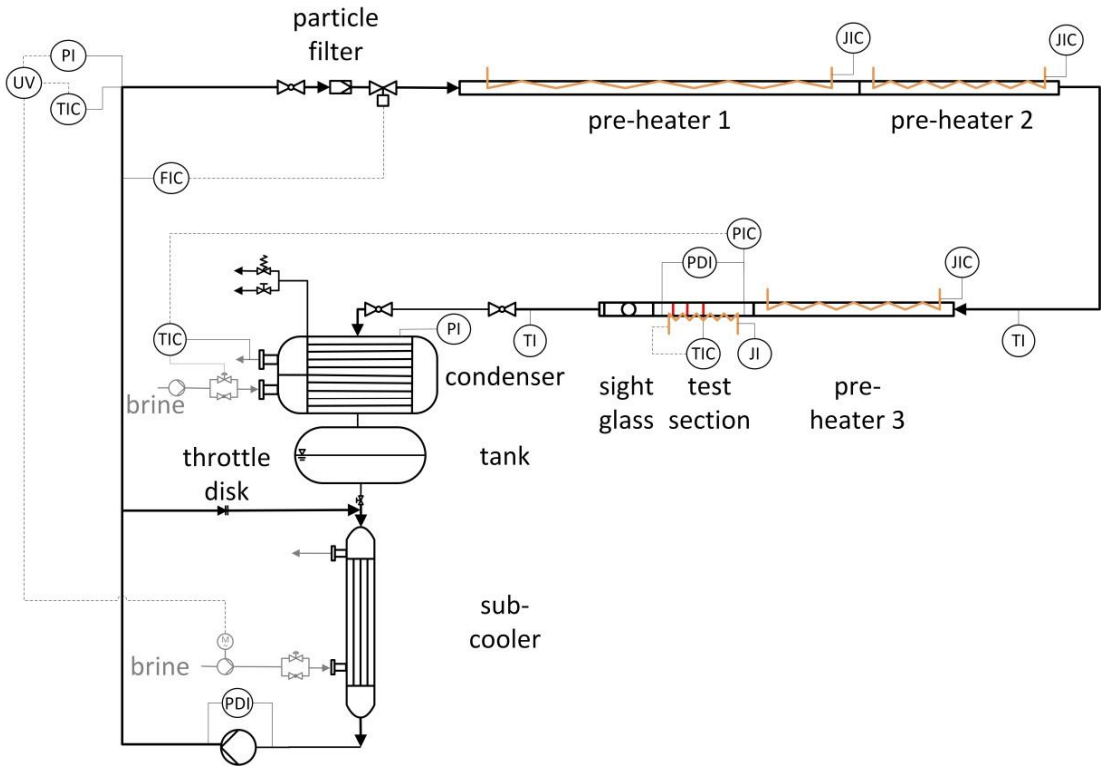

Fig. 1.
Process flow diagram of the flow boiling test facility.

The heat transfer coefficient was measured and recorded in steady state. Each reported data point represents an average of 40 data points recorded within 50 s. Both the average value and the standard deviation of these 40 data points are reported. Downstream of the test section and the sight glass, the vapor is re-liquefied in the condenser. Steady state was ensured by a start-up period of 40 minutes and a waiting time of at least 3 minutes after small changes until all parameters (averaged over 10 s to account for strongly fluctuating flow conditions) are constant within a specified range within three minutes ($\Delta\dot{m} < 1$ kg m^{-2} s^{-1}, $\Delta p < 0.02$ MPa, $\Delta\dot{x} < 0.01$, $\Delta\Delta p < 1$ mbar (10 ppi) or < 7 mbar (20 ppi)). To check the validity of these preset conditions, each recording was repeated after 5 minutes. The standard deviation may be higher than the preset conditions in case of strongly fluctuating flow conditions.

Test section

In Fig. 3 shows an axial view of the test section and the sight glass directly adjoining the test section. The test section is made of a brass tube with an inner diameter of 14.00 mm $\pm$0.01 mm and a mean arithmetic surface roughness of $R_A = 0.8 \cdot 10^{-6}$ m.

The thermal conductivity of the material of the test section in the temperature range of interest is 117 ± 8 W m^{-1} K^{-1} to 118 ± 8 W m^{-1} K^{-1}. The thermal conductivity was determined indirectly by measuring the thermal diffusivity, the heat capacity and the density of a material sample of the test section.

Six holes, drilled around the circumference at both the inlet and the outlet of the tube, connect the tube to two annular chambers integrated in inlet and outlet flange. The annular chamber ensures the correct measurement of an average static pressure of the two-phase flow, irrespective of the flow pattern. The inlet pressure tap is connected to a pressure transducer (Burster 8103-50). Inlet and outlet pressure taps are connected to a differential pressure transducer (Rosemount 3051C) measuring the pressure difference at a distance of $L = 247$ mm.

The heated zone of the tube is divided circumferentially into six segments by grooves. A graphite heating foil (SIGRAFLEX® F02012TH by SGL Carbon SE) heats each segment independently. The heating foil is separated from the test section electrically by a gap filler (TGF-R0500-SI by HALA Contec GmbH & Co. KG). To cramp the heating foil and the gap filler to obtain a uniform heating, they were fixed with three polyoxymethylene shells and staggered hose clamps. The graphite heating foils were electrically contacted by high current test probes (HSS-120 305 300 S 30 02 M by INGUN Prüfmittelbau GmbH).

The wall temperature is measured with thermocouples type E with a 304 SS sheath and a grounded junction. The cold junctions (electrically isolated by small glass tubes filled with silicon oil) of these thermocouples are tempered in a copper block immersed in a thermostat. The temperature of the cold junction is measured by a platinum resistance temperature detector (Pt100). The thermocouples were soldered into axial grooves in the tube wall. To obtain a uniform temperature distribution, thermocouple dummies were soldered into all grooves without thermocouples. The tips of the thermocouples end at three different planes of measurements (pm 1, pm 2, pm 3). The lengths between the beginning of the heating zone and the planes of measurement are 97.5 mm, 130.5 mm, and 163.5 mm, respectively. The distance between the thermocouple tip and the inner surface of the tube wall is 0.91$\pm$0.10 mm in pm 1, 0.89$\pm$0.10 mm in pm 2, and 0.88$\pm$0.10 mm in pm 3. Fig. 2 shows the cross-sectional view of the test section at a plane of measurement.

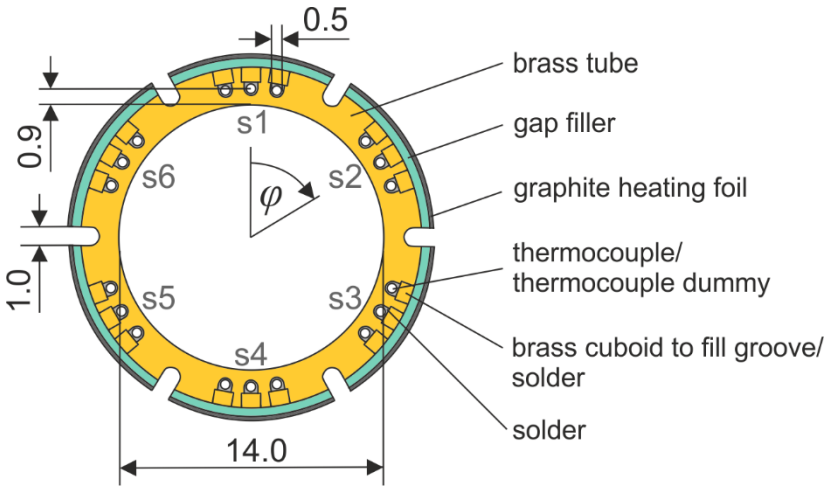

Fig. 2. Cross-sectional view of test section at a plane of measurement. The thermocouples in the plane of measurement 1, pm1, are located at angles $\varphi = 0°; 60°; 120°; 180°; 240°; 300°$. The angle is measured mathematically negative due to historical reasons.

This design of the test section allows two different boundary conditions to be set. On the one hand, the power of the individual segments can be controlled in such a way that the wall temperature is the same in all segments (constant wall temperature, data set identifier "T"). On the other hand, the same power can be applied to all segments (constant wall heat flux, data set identifier "q").

The copper sponge to be examined was inserted into the test section, see Fig. 3 for 10 ppi sponge and Fig. 4 for 20 ppi sponge, with a clearance fit of <70 µm. Due to manufacturing constraints, the sponge is composed of several short pieces. The copper sponge is framed by a plastic sponge in case of the 10 ppi sponge. The plastic sponge was inserted into the sight glass and the rest of the test section. A coarse sieve adjoining the sight glass provides fixation of the sponge. The total length of the 10 ppi copper sponge samples, L_{Cu}, is 200.2 mm. This corresponds approximately to the heated length (195 mm). The sample diameter of the copper sponge, measured by a micrometer screw gauge with an extended measurement uncertainty of ±0.05 mm, is $13.96\ ^{+0.02}_{-0.03}$ mm (10 ppi) or $13.97\ ^{+0.02}_{-0.02}$ mm (20 ppi). The length filled with sponge upstream of the heated zone, $L_{\mathrm{e,h}}$, was 38 mm (10 ppi) or either 35 mm or 135 mm (20 ppi). In case of the 20 ppi sponge, the test section was also filled partially to investigate entrance effects. Table 1 gives an overview over the pieces of 20 ppi sponge integrated into the test section and related lengths.

Table 1.
Sponge samples filled into the test section (compare Fig. 4) as well as lengths upstream of the planes of measurement and the heated zone for the 20 ppi sponge.

data set identifier	length upstream of heated section, $L_{\mathrm{e,h}}$ / mm	length upstream of pm 1 ($L_{\mathrm{e,h}} + L_{\mathrm{pm1}}$) / mm	length upstream of pm 2 ($L_{\mathrm{e,h}} + L_{\mathrm{pm2}}$) / mm	length upstream of pm 3 ($L_{\mathrm{e,h}} + L_{\mathrm{pm3}}$) / mm	sponge samples
pm3	-	-	-	5.5	I-VI
pm2	-	-	22.5	55.5	I-VII
shortened	35	131	164	197	I-IVb
basis	135	231	264	297	I-XI

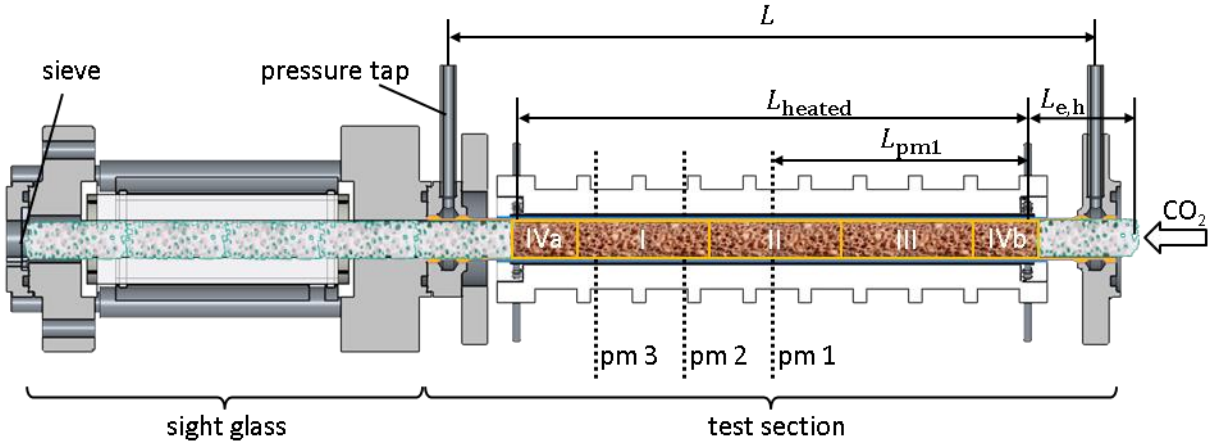

Fig. 3.
Axial view of the test section and the sight glass filled with 10 ppi copper and plastic sponge. Relevant lengths are the length between the pressure taps, L, the heated length, L_{heated}, the length upstream of the heated zone, $L_{e,h}$ and the length between the beginning of the heated zone and the planes of measurement L_{pm1}, L_{pm2},. L_{pm3}. For the sake of clarity, only L_{pm1} is shown.

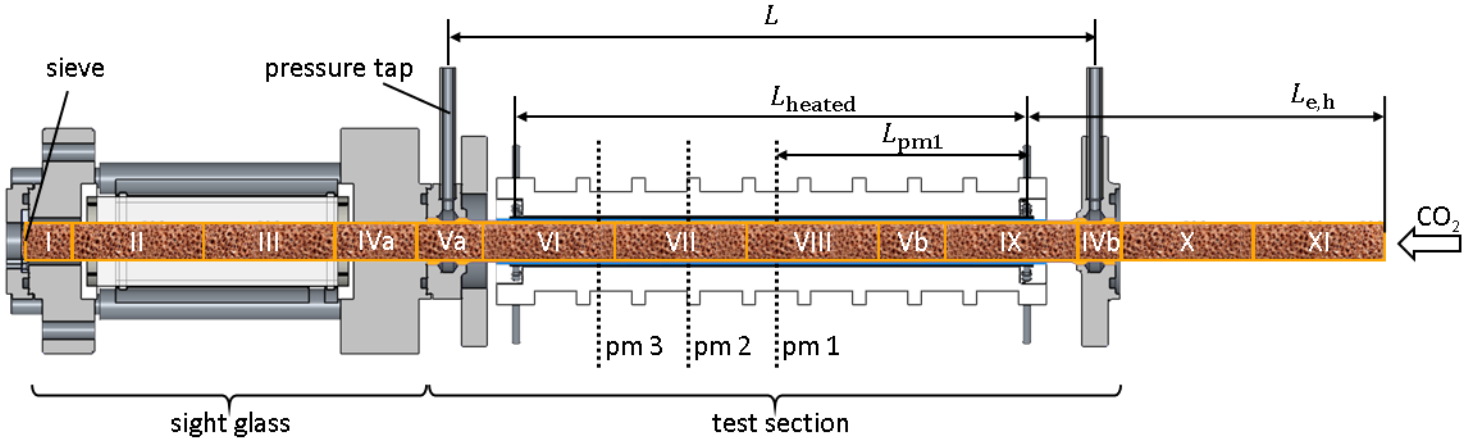

Fig. 4.
Axial view of the test section and the sight glass filled with 20 ppi copper sponge. Relevant lengths are the length between the pressure taps, L, the heated length, L_{heated}, the length upstream of the heated zone, $L_{e,h}$ and the length between the beginning of the heated zone and the planes of measurement L_{pm1}, L_{pm2},. L_{pm3}. For the sake of clarity, only L_{pm1} is shown.

Data reduction

The heat transfer coefficient, $\alpha_{i,j}$, of each segment j ($j = 1,2 \dots 6$) in the plane of measurement i ($i = 1,2,3$) is calculated by Eq. (1) taking into account the heat flux in the segment, $\dot{q}_j$, the temperature at the tube's inner wall, $T_{\mathrm{w},i,j}$ and the saturation temperature of the respective plane of measurement, $T_{\mathrm{sat},i}$.

$$\alpha_{i,j} = \frac{\dot{q}_j}{T_{\mathrm{w},i,j} - T_{\mathrm{sat},i}(p_{\mathrm{LV},i})} \tag{1}$$

The circumferentially averaged heat transfer coefficient is calculated in pm 1 by taking into account the mean heat flux, and the mean wall temperature.

$$\alpha_1 = \frac{\frac{1}{6}\sum_j \dot{q}_j}{\frac{1}{6}\sum_j T_{\mathrm{w},1,j} - T_{\mathrm{sat},1}(p_{\mathrm{LV},1})} \tag{2}$$

The heat flux, $\dot{q}_j$, is calculated by dividing the total heat transferred to the test section (electric heating and parasitic heat transfer, $\dot{Q}_j = \dot{Q}_{\mathrm{el},j} + \dot{Q}_{\mathrm{p},j}$,) by the tube's inner surface area in the heated zone corresponding to segment j.

$$\dot{q}_j = \frac{\dot{Q}_{\mathrm{el},j} + \frac{1}{6}\dot{Q}_{\mathrm{p}}}{\frac{2\pi}{6} \cdot D_{\mathrm{i}} \cdot L_{\mathrm{heated}}} \tag{3}$$

The heat supplied to segment j , $\dot{Q}_{\mathrm{el},j}$, is calculated from the power supplied to the heating foils taking into account the reactive power in the connection lines. The heat transfer from the environment, $\dot{Q}_{\mathrm{p}}$, is estimated by means of the thermal transmittance, which was determined at vacuum conditions and validated by single-phase measurements. The heat transfer area of one segment is related to the tube's inner diameter, D_{i} and the heated length, L_{heated}.

The temperature at the tube's inner wall in each segment j and plane of measurement i, $T_{\mathrm{w},i,j}$ is determined by extrapolating from the temperature measured by the thermocouples in the tube wall $T_{\mathrm{tc,i,j}}$.

$$T_{w,i,j} = T_{\mathrm{tc,i,j}} - \frac{6 \cdot \dot{Q}_j \cdot \ln\left(\frac{D_{\mathrm{tc},i}}{D_{\mathrm{i}}}\right)}{2\pi \cdot L_{\mathrm{heated}} \cdot \lambda_{\mathrm{ts}}} \tag{4}$$

Eq. (4) considers the heat transferred through the respective segment, $\dot{Q}_j = \dot{Q}_{\mathrm{el},j} + \frac{1}{6}\dot{Q}_{\mathrm{p}}$, the diameter related to the thermocouple tips in each plane of measurement i, $D_{\mathrm{tc},i}$, the tube's inner diameter, D_{i}, the heated length, L_{heated} and the thermal conductivity of the test section, λ_{ts}.

The saturation temperature is calculated at each plane of measurement from the pressure in that plane using the equation of state of CO_2 by Span and Wagner [7]. As the change in vapor quality in the test section is small, the pressure is estimated by linear interpolation between the two pressure taps according to Eq. (5).

$$p_{\mathrm{sat},i} = p_{\mathrm{ts,in}} + \frac{L_i}{L}\Delta p \tag{5}$$

Here, $p_{\mathrm{sat,ts,in}}$ is the static pressure measured at the inlet of the test section, L_i the distance between the inlet pressure tap and the plane of measurement i, L the distance between the two pressure taps and Δp the measured pressure difference.

The mass flux, $\dot{m}$, is related to the cross-sectional area of the empty tube.

The mean vapor quality (at each plane of measurement) is calculated by means of an enthalpy balance between the entrance of the test conduit (in), at which the refrigerant is subcooled and the respective plane of measurement (i) assuming thermodynamic equilibrium. The enthalpy at the entrance of the test conduit is a function of both pressure and temperature at this point, $h_{\mathrm{L,in}} = f(T_{\mathrm{in}}, p_{\mathrm{in}})$. The liquid enthalpy and the enthalpy of vaporization in the plane of measurement, $h_{\mathrm{L},i}$ and $\Delta h_{\mathrm{LV},i}$ are a function of the saturation pressure, $p_{\mathrm{LV},i}$ only.

$$\dot{x}_i = \frac{\sum \dot{Q} - \left(h_{\mathrm{L},i} - h_{\mathrm{L,in}}\right) \cdot \dot{m}}{\Delta h_{\mathrm{LV},i} \cdot \dot{m}} \tag{6}$$

The heat supplied by the preheaters and the respective part of the test section as well as parasitic heat transfer from the environment through the insulation are taken into account, i.e. $\sum \dot{Q} = \sum \dot{Q}_{\mathrm{el}} + \sum \dot{Q}_{\mathrm{p}}$. Similar to the heat supply in the test section, the reactive power in the connection lines and the thermal transmittance of the insulation of the preheaters are considered.

Measurement uncertainty

The evaluation of the uncertainty of measurement follows the “Guide to the expression of uncertainty in measurement” (GUM) [8]. The standard uncertainties of the measurands, i.e. temperatures, power, pressures, differential pressure, and mass flow, are estimated by means of a type B evaluation. The individual evaluation is based on the manufacturer’s specifications of the measurement device or calibration device, on preliminary tests, or – for the temperature distribution in the test section – on numerical calculations. A similar procedure is applied to estimate the standard uncertainty of geometrical and material properties such as the thermal conductivity of the tube wall, the thermal transmittance of the insulation or the dimension of the test section. Table 2 lists the standard uncertainties of the measurands. Deviations from previous publications are due to a revaluation.

Table 2.
Instrument standard uncertainties (k= 1).

instrument	$\sigma\ (k = 1)$	notes
digital power meter	±0.05% of reading	according to calibration
thermocouple type E (test section)	±0.14 K	mainly due to geometrical imperfection of the test section and irregular heat transfer, determined by numerical simulation
thermocouple type E (insulation test section)	±0.02 K	with external cold junction, calibrated, uncertainty of calibration standard and calibration procedure
thermocouple type K (insulation)	< ±0.4 K	with internal cold junction, IEC-60584-1 [9], checked by comparison to calibration standard
resistance thermometer (Pt100)	±0.02 K	uncertainty of calibration standard and calibration procedure
pressure transducer	0.018 bar ±0.008% of reading	uncertainty of calibration standard and calibration procedure
differential pressure transducer	±0.4 mbar	uncertainty of calibration standard and calibration procedure
mass flow meter	±0.15% of reading; ±0.02% of range	manufacurer's specification

The expanded combined standard uncertainty with a coverage factor of k=2 describing a confidence level of 95% is calculated from these basic standard uncertainties by error propagation and is reported for the vapor quality, the mass flux, the saturation temperature, the heat fluxes and the heat transfer coefficients.

To demonstrate the reproducibility of the heat transfer coefficient, data were recorded by different persons on different days at intervals of several weeks for the same operating conditions (data set identifier "rep"). These data coincide within the scope of the measurement uncertainty.

Sponges

This paragraph is the same as in the article accompanying the data sets on the pressure drop in a horizontal tube filled with metal sponge [6]. The only additional information is the two-phase thermal conductivity of the sponge samples filled with stagnant air, $\lambda_{2\mathrm{Ph},0}$. Two-phase refers to the solid and the fluid phase in this case.

The investigated copper sponges were obtained from the Fraunhofer Institute for Manufacturing Technology and Advanced Materials (IFAM) in Dresden (compare Fig. 5). Several blocks were made by replication technique [10] using a polyurethane template.

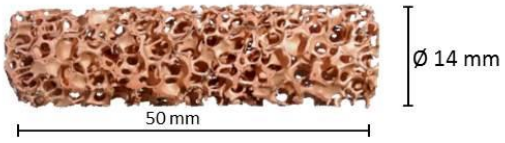

Fig. 5.
Photograph of one of the copper sponge samples (10 ppi), which were integrated in test section.

Table 3 and Table 4 provide an overview of averaged properties, their uncertainty and variation, as well as the methods for characterizing the copper samples used. The total porosity was determined for each sample. The strut diameter was measured halfway between two nodes, corresponding to the thinnest diameter of the strut. The window diameter was determined by averaging the major and minor axis, as the windows are ellipsoidal and feature a ratio of major to minor axis of approximately 1.5.

Table 3.
Geometric characteristics of the 10 ppi copper sponge samples integrated into the test section. Values are averaged for the samples. The maximum deviation between any sample's property and its mean value is given to assess their homogeneity. The measurement uncertainty (k=2) according to GUM [8] of each method is given if applicable. Standard deviation of multiple measurements of the same structure, s, and standard deviation of the mean s_x, are given if applicable.

property	averaged value and maximum deviation	method/instrument	uncertainty of method / standard deviation
nominal cell density	10 ppi	customary designation of template provider	-
total porosity, Ψ_t	sample I-IV: $90.7\ ^{+0.4}_{-0.3}$ %	direct method density of pure copper: 8.94 kg m^{-3} [11]	$2\sigma = \pm 0.07\%$
	sample V: 90.7%		
open porosity, Ψ_o	$87.6\ ^{+0.2}_{-0.2}$ %	gas pycnometry @ CVT, KIT (AccuPyc Pycnometer 1330)	$2\sigma = \pm 0.41\%$
	sample V: 85.5%	reconstruction of µCT scan (ZEISS Xradia 520 Versa, resolution 15 µm, test specimen: $h = 50$ mm; $d = 14$ mm)	
secondary porosity ($V_{\text{secondary pores}}/V_s$)	8.4%	digital image processing of light optical micrographs of metallographic specimen	$2\sigma = \pm 3.4\%$
mean strut diameter, d_s	sample I-III: 450 µm	optical microscope	$s_x = 16$ µm; $s = 103$ µm
	sample IV, V: 429 µm		$s_x = 24$ µm; $s = 132$ µm
mean window diameter, d_w	sample I-III: 1561 µm	optical microscope	$s_x = 63$ µm; $s = 332$ µm
	sample IV, V: 1580 µm		$s_x = 75$ µm; $s = 396$ µm
specific surface area, $S_v = \frac{A}{V_{cylinder}}$	sample V: 952 m^{-1}	reconstruction of µCT scan (ZEISS Xradia 520 Versa, resolution 15 µm, test specimen: h = 50 mm; d = 14 mm)	
thermal conductivity, $\lambda_{2\text{Ph},0}$	2.7 W m^{-1} K^{-1}	plate apparatus with monotonic, unidirectional heat flux and comparison to reference specimen (method as described by Dietrich et al. [12])	$2\sigma = \pm 1.2$ W m^{-1} K^{-1}
thermal conductivity, $\lambda_{2\text{Ph},0}$	1.66 W m^{-1} K^{-1}	plate apparatus with monotonic, unidirectional heat flux and comparison to reference specimen, measured @ Fraunhofer IFAM	$\sigma \pm 0.15$ W m^{-1} K^{-1}

Table 4.
Geometric characteristics of the 20 ppi copper sponge samples integrated into the test section. Values are averaged for the samples. The maximum deviation between any sample's property and its mean value is given to assess their homogeneity. The measurement uncertainty (k=2) according to GUM [8] of each method is given if applicable. Standard deviation of multiple measurements of the same structure, s, and standard deviation of the mean s_x, are given if applicable.

property	averaged value and maximum deviation	method/instrument	uncertainty of method/ standard deviation
nominal cell density	20 ppi	customary designation of template provider	-
total porosity, Ψ_t	sample I-VII: $89.7\ ^{+0.8}_{-0.4}$ %		$2\sigma = \pm 0.07\%$
	sample VIII: 89.9%		
open porosity, Ψ_o	sample VIII: 86.8%	gas pycnometry @ CVT, KIT (AccuPyc Pycnometer 1330)	$2\sigma = \pm 0.41\%$
	sample VIII: 84.5%	reconstruction of µCT scan (ZEISS Xradia 520 Versa, resolution 15 µm, test specimen: $h = 50$ mm; $d = 14$ mm)	
secondary porosity ($V_{\text{secondary pores}}/V_s$)	8.4%	digital image processing of light optical micrographs of metallographic specimen	$2\sigma = \pm 3.4\%$
mean strut diameter, d_s	sample II-IV,X: 246 µm	optical microscope	$s_x = 10$ µm; $s = 56$ µm
	sample VI-VIII: 275 µm		$s_x = 14$ µm; $s = 72$ µm
mean window diameter, d_w	sample II-IV,X: 1130 µm	optical microscope	$s_x = 58$ µm; $s = 273$ µm
	sample VI-VIII: 1027 µm		$s_x = 53$ µm; $s = 238$ µm
specific surface area, $S_v = \frac{A}{V_{cylinder}}$	sample X: 1375 m^{-1}	reconstruction of µCT scan (ZEISS Xradia 520 Versa, resolution 15 µm, test specimen: h = 50 mm; d = 14 mm)	
thermal conductivity, $\lambda_{2\text{Ph},0}$	4 W m^{-1} K^{-1}	plate apparatus with monotonic, unidirectional heat flux and comparison to reference specimen (method as described by Dietrich et al. [12])	$2\sigma = \pm$ 1.2 W m^{-1} K^{-1}

Table 5 provides an overview of averaged properties of the plastic sponge made of VisiJet® M2-RCL, an acrylate polymer, 3D printed by KSP GmbH. This sponge was inserted upstream and downstream of the 10 ppi copper sponge samples. The length of the plastic sponge amounts to 18.9% of the distance between the pressure taps. At the time of 3D printing of the plastic sponges, no µCT scan of the copper sponge was available. Hence, a µCT scan of a 10 ppi ceramic sponge was used to create the 3D model for printing the plastic sponge. The ceramic sponge model was chosen as was available with the necessary high quality. The geometric properties of this ceramic sponge are comparable to those of the copper sponge. This 3D model first had to be edited manually to ensure printability, i.e. internal pores were closed with CAD software and artefacts were cleaned up. The geometric properties of the plastic sponge, listed in Table 5 were derived from this 3D CAD model and checked with the optical microscope after use in the

test section. The struts seem to be slightly thicker than specified by the 3D CAD model. The real macroscopic surface area therefore probably deviates slightly from the macroscopic surface area determined from the 3D CAD model.

Table 5.
Geometric characteristics of the plastic sponge samples integrated into the test section. Values are derived from 3D CAD model and compared to values obtained by optical microscopy (*). Standard deviation, s, and standard deviation of the mean, s_x, are given if applicable.

property	averaged value	comment
total porosity, $\Psi_t\ (=\Psi_0)$	85.5%	
mean strut diameter, d_s	580 µm	s_x= 20 µm s = 142 µm
	650 µm (*)	s_x= 18 µm (*) s = 87 µm (*)
mean window diameter, d_w	2380 µm	s_x= 154 µm s = 598 µm
	2000 µm (*)	s_x= 117 µm (*) s = 523 µm (*)
macroscopic surface area, $S_{v,\mathrm{incl}}$	580 m^{-1}	including the fraction of the cylinder shell surface covered by the porous structure, voxel size of underlying µCT-scans: 0.056 mm, coarsened with triangulation length: 0.13 mm
macroscopic surface area, $S_{v,\mathrm{excl}}$	530 m^{-1}	excluding surface area of intersection with cylinder $S_{v,\mathrm{excl}} = \frac{A_{\mathrm{incl}} - \Psi_t \cdot A_{\mathrm{cylinder}}}{V_{\mathrm{cylinder}}}$
sample diameter	13.9 mm	
sample length	36.6 mm	

Acknowledgments

The authors would like to thank the German Research Foundation (DFG, Deutsche Forschungsgemeinschaft) for their financial support [grant number 245385027]. Furthermore, we acknowledge the support of the Institute of Chemical Process Engineering (CVT), KIT for porosity measurements (gas pyconometry) and of the Institute for Applied Materials – Materials for Electrical and Electronic Engineering (IAM-WET), KIT for computed tomography scans. We further acknowledge the contribution of Anna-Maria Eckel, who characterized the geometry and the thermal conductivity of the copper sponges, and of Isabel Aliaño Ramos, who supported the measurement of the 20 ppi data.

Funding

This work was supported by the German Research Foundation (DFG, Deutsche Forschungsgemeinschaft) [grant number 245385027].

References

[1] A.E. Schael, M. Kind, Flow pattern and heat transfer characteristics during flow boiling of CO_2 in a horizontal micro fin tube and comparison with smooth tube data, Int. J. Refrig., 28 (2005) 1186–1195.

[2] A.E. Schael, Über das Strömungsverdampfen von CO_2 im glatten und innen berippten Rohr - Hydrodynamik, Wärmeübergang, Druckverlust, Ph.D. Thesis, Universität Fridericiana Karlsruhe (TH), Karlsruhe, 2009.

[3] M. Wetzel, B. Dietrich, T. Wetzel, Influence of oil on heat transfer and pressure drop during flow boiling of CO_2 at low temperatures, Exp. Therm Fluid Sci., 59 (2014) 202–212. doi:10.1016/j.expthermflusci.2014.05.001.

[4] M. Wetzel, Influence of fully miscible lubrication oil on flow boiling of CO_2 inside horizontal evaporator tubes, Ph.D. Thesis, Karlsruher Institut für Technologie, Karlsruhe, 2017.

[5] S. Weise, M. Wetzel, B. Dietrich, T. Wetzel, Influence of fully miscible lubricating oil on the pressure drop during flow boiling of CO_2 inside an enhanced tube, Exp. Therm Fluid Sci., 81 (2017) 223–233. doi:10.1016/j.expthermflusci.2016.09.018.

[6] S. Weise, S. Klein, T. Wetzel, B. Dietrich, Pressure drop data of two-phase flow in a horizontal tube filled with metal sponge, KITopenData, 2018, https://publikationen.bibliothek.kit.edu/1000085053. doi:10.5445/IR/1000085053.

[7] R. Span, W. Wagner, A new equation of state for carbon dioxide covering the fluid region from the triple-point temperature to 1100 K at pressures up to 800 MPa, J. Phys. Chem. Ref. Data, 25 (1996) 1509–1596. doi:10.1063/1.555991.

[8] JCGM 100:2008, Evaluation of measurement data—Guide to the expression of uncertainty in measurement, GUM 1995 with minor corrections, https://www.bipm.org/utils/common/documents/jcgm/.

[9] IEC 60584-1, Thermocouples - Part 1: EMF specifications and tolerances, 3.0th ed., Geneva, 17.200.20, 2013.

[10] P. Quadbeck, K. Kümmel, R. Hauser, G. Standke, J. Adler, G. Stephani, Open cell metal foams – Application-oriented structure and material selection, in: Proc. of CellMat, 2010.

[11] Deutsches Kupfer-Institut, DKI Werkstoff-Datenblätter, 2005.

[12] B. Dietrich, G. Schell, E.C. Bucharsky, R. Oberacker, M.J. Hoffmann, W. Schabel, M. Kind, H. Martin, Determination of the thermal properties of ceramic sponges, Int. J. Heat Mass Transfer, 53 (2010) 198–205. doi:10.1016/j.ijheatmasstransfer.2009.09.041.